
Article:
Cannon, DT, Rodewohl, L, Adams, V et al. (2 more authors) (2019) Skeletal myofiber VEGF deficiency leads to mitochondrial, structural and contractile alterations in mouse diaphragm. Journal of Applied Physiology, 127 (5). pp. 1360-1369. ISSN 8750-7587

https://doi.org/10.1152/japplphysiol.00779.2018

Skeletal myofiber VEGF deficiency leads to mitochondrial, structural, and contractile alterations in mouse diaphragm

Daniel T Cannon[1]*, Lukas Rodewohl[2]*, Volker Adams[3], Ellen C Breen[4], T Scott Bowen[5]

[1]School of Exercise & Nutritional Sciences, San Diego State University
[2]Department of Internal Medicine and Cardiology, Universität Leipzig Herzzentrum
[3]Department of Internal Medicine and Cardiology, Technische Universität Dresden
[4]Department of Medicine, University of California, San Diego
[5]School of Biomedical Sciences, Faculty of Biological Sciences, University of Leeds
*equal contribution

Author Contributions

Concept and design: DTC, ECB, TSB. Data acquisition: DTC, LR, ECB, TSB. Data analysis: DTC, LR, TSB. Data interpretation: DTC, LR, VA, ECB, TSB. Figure preparation: DTC, LR, TSB. Manuscript drafting: DTC, LR, TSB. Critical Revision: DTC, LR, VA, ECB, TSB. All authors approved the final version.

Corresponding Author
T. Scott Bowen
School of Biomedical Sciences
University of Leeds, Leeds, LS2 9JT
t.s.bowen@leeds.ac.uk

Running title: Myofiber VEGF deletion induces diaphragm dysfunction

Key words: diaphragm, muscle, fatigue, mitochondria

Abstract

Diaphragm dysfunction accompanies cardiopulmonary disease and impaired oxygen delivery. Vascular endothelial growth factor (VEGF) regulates oxygen delivery through angiogenesis, capillary maintenance, and contraction-induced perfusion. We hypothesized that myofiber-specific VEGF deficiency contributes to diaphragm weakness and fatigability. Diaphragm protein expression, capillarity and fiber morphology, mitochondrial respiration and hydrogen peroxide (H_2O_2) generation, and contractile function were compared between adult mice with conditional gene ablation of skeletal myofiber VEGF (SkmVEGF$^{-/-}$; n=12) and littermate controls (n=13). Diaphragm VEGF protein was ~50 % lower in SkmVEGF$^{-/-}$ than littermate controls (1.45±0.65 vs. 3.04±1.41 pg/total protein; P=0.001). This was accompanied by an ~15% impairment in maximal isometric specific force (F[1,23] = 15.01, P=0.001) and a trend for improved fatigue resistance (P=0.053). Mean fiber cross-sectional area and type I fiber cross-sectional area were lower in SkmVEGF$^{-/-}$ by ~40 % and ~25% (P<0.05). Capillary-to-fiber ratio was also lower in SkmVEGF$^{-/-}$ by ~40% (P<0.05), thus capillary density was not different. Sarcomeric actin expression was ~30% lower in SkmVEGF$^{-/-}$ (P<0.05), while myosin heavy chain and MAFbx were similar (measured via immunoblot). Mitochondrial respiration, citrate synthase activity, PGC-1α, and HIF-1α were not different in SkmVEGF$^{-/-}$ (P>0.05). However mitochondrial-derived reactive oxygen species (ROS) flux was lower in SkmVEGF$^{-/-}$ (P=0.0003). In conclusion, myofiber-specific VEGF gene deletion resulted in a lower capillary-to-fiber ratio, type I fiber atrophy, actin loss, and contractile dysfunction in the diaphragm. In contrast, mitochondrial respiratory function was preserved alongside lower ROS generation, which may play a compensatory role to preserve fatigue resistance in the diaphragm.

Abstract word count: 244 (250 max).

New and Noteworthy (75 words max).

Diaphragm weakness is a hallmark of diseases where oxygen delivery is compromised. Vascular endothelial growth factor (VEGF) modulates muscle perfusion, however it remains unclear whether VEGF deficiency contributes to the onset of diaphragm dysfunction.

Conditional skeletal myofiber VEGF gene ablation impaired diaphragm contractile function and resulted in type I fiber atrophy, a lower number of capillaries per fiber, and contractile protein content. Mitochondrial function was similar and ROS flux was lower. Diaphragm VEGF deficiency may contribute to the onset of respiratory muscle weakness.

Introduction

Respiratory muscle weakness develops in many clinical conditions, such as acute critical illness, chronic cardiopulmonary disorders, and in aging (23). In particular, impairments to the main muscle of respiration, the diaphragm, contributes substantially to pulmonary complications and poor clinical outcomes in patients (18, 33). However, the mechanisms that induce diaphragm weakness and effective rescue treatments remain poorly resolved. Most clinical disorders associated with diaphragm dysfunction are characterized by abnormal microvasculature and O_2 delivery (49) (e.g., critical illness, chronic heart failure, chronic obstructive pulmonary disease; COPD). Abnormalities in the O_2 transport system may be a key mechanism for triggering the onset of diaphragm weakness (23). Vascular endothelial growth factor (VEGF) is a transmembrane glycoprotein that is requisite for blood vessel development and maintenance in all mammalian organs. VEGF is a family of 5 growth factors (VEGF-A, VEGF-B, VEGF-C, VEGF-D, PGF) that have various roles during embryonic/adult tissue development and maintenance. However, VEGF-A (referred hereafter as VEGF) is the most predominant form in the majority of tissues/organs in adults. In addition to signal transduction for angiogenesis, VEGF is critical for stem cell recruitment, maintenance of vulnerable barriers (i.e. lung, nephron and kidney cells), and protection of neural tissue (10, 51).

VEGF plays a critical role in locomotor skeletal muscle structure and function and these variables impact whole-organism functions, such as exercise tolerance (26, 50). Further, skeletal muscle remodeling following exercise training is highly dependent on VEGF being properly expressed in a variety of tissues, including skeletal myofibers (16, 25). VEGF is down-regulated in leg muscle samples taken from patients with diseases characterized by abnormalities in O_2 supply, such as in COPD (5). In contrast, the role of VEGF expression in the diaphragm remains poorly characterized and whether low VEGF contributes to diaphragm contractile dysfunction is unknown. Interestingly, in rats undergoing mechanical ventilation where the diaphragm

undergoes arrest to induce severe fiber weakness, VEGF is reduced by around two-fold (11, 17). However in conditions with high mechanical respiratory loading, such as COPD (2) or under hypoxic conditions (46), VEGF mRNA expression in the diaphragm is elevated. Thus, it seems that in conditions characterized by diaphragm disuse such as in critical illness, a reduction in VEGF expression may contribute towards respiratory muscle weakness. The mechanisms that underpin diaphragm dysfunction have been suggested to include fiber atrophy (due to an imbalance in protein synthesis/degradation), elevated reactive oxygen species (ROS), an oxidative to glycolytic fiber type transition, and mitochondrial dysfunction (23, 41).

Based upon the importance of VEGF in locomotor skeletal muscle during adaptation to exercise training and various pathologies, we aimed to measure whether VEGF deficiency modulates diaphragm contractile function, capillarity, fiber structure, and mitochondrial bioenergetics. Given that diaphragm tissue demonstrates a high degree of cellular abnormalities in a variety of diseases (6, 8, 9, 31, 32), we hypothesized that low myofiber VEGF impairs diaphragm contractile function and is accompanied by fiber remodeling and mitochondrial functional deficits including capillary regression, fiber atrophy, shifts from oxidative to glycolytic fiber types, and reduced maximal mitochondrial oxygen flux with increased ROS generation.

Materials and Methods

Animals and Study Design

We measured diaphragm biochemistry, structure, and contractile function in adult mice with conditional deletion of the VEGF-A gene in skeletal myofibers (SkmVEGF$^{-/-}$). To achieve this, we maintained and bred mice homozygous for the VEGFLoxP transgene (22) with mice heterogeneous for HSA-Cre-ER^{T2} (44). Animals were housed in a pathogen-free vivarium in plastic cages, with a 12:12 hr light:dark cycle, and fed a standard chow diet (Harlan Tekland 8604, Madison, WI) with water ad libitum. Conditional myofiber-specific deletion of VEGF was initiated at 10 weeks of age (body weight ~20 g) using a tamoxifen-inducible HSA-Cre-ER^{T2} system in the VEGFLoxP mice on a C57BL/6J background (16). Male SkmVEGF$^{-/-}$ mice (n=12) were compared to floxed wild type (WT) controls (n=13) that did not express cre recombinase (HSA-Cre-ER$^{T2-/-}$). All mice received tamoxifen (1 mg/day i.p.) for 5 consecutive d (D0-D4). Following completion of the tamoxifen treatment period and sufficient time for VEGF expression to be decreased, mice were anesthetized on day 21 (D21) with inhaled isoflurane vaporized in 100% O_2 and killed through removing the major organs. Our protocol was approved by the University of California, San Diego, Animal Care and Use Committee and was conducted in accordance to guidelines outlined by the NIH's Guide for the Care and Use of Laboratory Animals.

Genotyping

The presence of HSA-Cre-ER^{T2} transgene was measured by PCR from tail DNA and forward 5′-CTAGAGCCTGTTTTGCACGTTC-3′ and reverse primers 5′-TGCAAGTTGAATAACCGGAAA-3′. The conditions during cycling were a 2-min polymerase activation incubation at 95℃, 35 cycles of 30 s denaturation at 94℃, 30 s annealing at 52.1℃, 60 s elongation at 72℃, followed by one 8-min elongation at 72℃.

Diaphragm Dissection and Contractile Function

The diaphragm was excised through a laparotomy and thoracotomy. The right costal diaphragm muscle was divided for measurement of mitochondrial function and the remainder immediately snap-frozen in liquid N_2 for later biochemical analyses. The left costal diaphragm muscle was prepared in a Krebs-Hanseleit buffer solution (120.5 mM NaCl, 4.8 mM KCl, 1.2 mM $MgSO_4$, 1.2 mM NaH_2PO_4, 20.4 mM $NaHCO_3$, 1.6 mM $CaCl_2$, 10 mM dextrose, 1 mM pyruvate at a pH of 7.4) and a muscle bundle (~3 mg) connected from rib to central tendon was dissected, sutured (size 4.0), and mounted horizontally in a buffer-filled organ bath at room temperature equilibrated with 95%O_2-5%CO_2. The suture connected to the rib was secured to a hook in the organ bath while the tendon was tied to an adjustable-length force transducer (Model 920CS, DMT, Aarhus, DK). The muscle was stimulated via platinum electrodes with a supramaximal current (500-ms train duration; 0.25-ms monophasic pulses) via a high-power stimulator (Model S88, Grass Medical Instruments, Quincy, MA). The muscle bundle was set at an optimal length equivalent to the maximal twitch force produced and a 15-min equilibration period followed. A force-frequency protocol was then performed at 1, 15, 30, 50, 80, 120, 150, and 300 Hz, respectively, separated with 1-min rest intervals. Following a 5-min period in which muscle length was measured using a digital micrometer, the muscle underwent a fatigue protocol over 5 min (40 Hz every 2 s with a 500-ms train duration). The muscle was subsequently detached, trimmed free from rib and tendon, blotted dry on filter paper, and weighed. Muscle force (N) was normalized to muscle cross-sectional area (cm^2) by dividing muscle mass (g) by the product of optimal length (cm) and estimated muscle density (1.06 g/cm^3) (13), which allowed specific force in N/cm^2 to be calculated.

Mitochondrial function

Dissected diaphragm tissue (~5-10 mg) was placed immediately in preservation solution at 4℃. Preservation medium (BIOPS) contained 10 mM Ca^{2+}EGTA buffer, 20 mM imidazole, 50 mM K^+-4-morpholineothanesulfonic acid (MES), 0.5 mM dithiothreitol, 6.56 mM $MgCl_2$, 5.77 mM ATP, 15

mM phosphocreatine and a pH of 7.1. Fiber bundles (each approximately 0.5 to 1 mg) were transferred to a plastic culture dish and kept in BIOPS at 4℃. The bundles were mechanically separated using sharp forceps and a dissection microscope (Leica, DE). The bundles were permeabilized with a 30 min incubation in saponin (50 µg/ml) dissolved in BIOPS at 4℃. Tissues were washed of saponin for 10 min in respiration medium at 4℃. Fiber bundles were weighed to the nearest µg using an ultrabalance (UMX2, Mettler-Toledo, Greifensee, CH) and transferred into a calibrated respirometer (Oxygraph 2k, OROBOROS INSTRUMENTS, Innsbruck, AT) containing 2 ml of media in each chamber. Respirometry and fluorometry was performed in duplicate at 37℃ in stirred media (MiR05+Cr) containing 0.5 mM EGTA, 3 mM $MgCl_2$, 60 mM K-lactobionate, 20 mM taurine, 10 mM KH_2PO_4, 20 mM HEPES, 110 mM sucrose, 20 mM creatine, and 1 g/l BSA essentially fatty acid free, adjusted to pH 7.1. [O_2] in the media was kept between 300–500 µM.

A substrate-uncoupler-inhibitor-titration (SUIT) protocol (37) included: 10 mM glutamate and 2 mM malate to support electron entry through complex I (GM; 'LEAK' state), 5 mM ADP to stimulate oxidative phosphorylation ('OXPHOS_CI' state), 10 mM succinate to maximize convergent electron flux at the Q-junction (ADP+S; OXPHOS_CI+II), carbonyl cyanide-3-chlorophenylhydrazone (CCCP) titrated in 0.5 µM steps to achieve maximal uncoupled respiration for measurement of electron transport system capacity ('ETS' state), 0.5 µM rotenone to inhibit complex I (Rot; ETS_CII). The flux control ratio for OXPHOS was calculated as (OXPHOS_CI/ETS) and (OXPHOS_CI+II/ETS). OXPHOS coupling efficiency was calculated as (1-LEAK/OXPHOS_CI+II). The substrate control ratio for succinate was calculated as (OXPHOS_CI+II/OXPHOS_CI).

In parallel to respirometry, the green fluorescence-sensor of the O2k-Fluo LED2-Module (OROBOROS) and the Amplex UltraRed assay was used to measure hydrogen peroxide (H_2O_2)

production during of the respiratory states – an index of total mitochondrial ROS production (27). Amplex UltraRed (AmR; 10µM), horseradish peroxidase (HRP; 1 U/mL) and superoxide dismutase (SOD; 5 U/mL) were injected prior to addition substrates. AmR is oxidized by H_2O_2 in the presence of HRP and allows for an excitation/emission at 563 and 587 nm. [H_2O_2] was determined by calibrating to a series of injections of 0.1 µM H_2O_2 using a 40uM stock solution made fresh daily.

Muscle Biochemistry

VEGF protein in diaphragm tissue was quantified by ELISA and normalized to total protein, in accordance to the manufacturer's instructions (VEGF Mouse ELISA, R&D Systems, La Jolla, CA). For western blotting, frozen muscle samples were homogenized in relaxing buffer (90 HEPES, 126 KCl, 36 NaCl, 1 MgCl, 50 EGTA, 8 ATP, 10 creatine phosphate, in mmol/L at pH 7.4) containing a protease inhibitor mix (Inhibitor mix M, Serva, Heidelberg, Germany), and sonicated for 10 cycles (Sonoplus GM70, Bandelin Electronics, Berlin Germany), with protein content of the homogenate subsequently determined (BCA assay, Pierce, Bonn, Germany). Citrate synthase activity (a marker of mitochondrial content) was assessed at room temperature, as previously described (6, 8, 9, 31, 32). Diaphragm homogenates (5 - 20 µg) mixed with loading buffer (126 mM Tris-HCl, 20% glycerol, 4% SDS, 1.0% 2-mercaptoethanol, 0.005% bromophenol blue; pH 6.8) were separated by SDS-polyacrylamide gel electrophoresis. Proteins were transferred to a polyvinylidene fluoride membrane (PVDF) and incubated overnight at 4℃ wi th the following primary antibodies for the contractile proteins of myosin heavy chain (MyHC; 1/1000, Sigma-Aldrich, Taufkirchen, Germany), and sarcomeric actin (1/500; Sigma-Aldrich, Taufkirchen, Germany), the signaling proteins of PGC1-α (1/200, Santa Cruz, Heidelberg, Germany) and HIF1-α (1/200, Santa Cruz, Heidelberg, Germany), and the stress-related proteins MAFbx (1/2000; Eurogentec, Seraing, Belgium) and NADPH oxidase subunit $gp91^{phox}$ (1/1000; Abcam, Cambridge, UK). Membranes were subsequently incubated with a horseradish peroxidase-

conjugated secondary antibody and specific bands visualized by enzymatic chemiluminescence (Super Signal West Pico, Thermo Fisher Scientific Inc., Bonn, Germany) and densitometry quantified using a 1D scan software package (Scanalytics Inc., Rockville, USA). Blots were then normalized to the loading control GAPDH (1/30000; HyTest Ltd, Turku, Finland), which we confirmed was not different between experimental groups. All data are presented as fold change relative to control group.

Histology

Liquid-nitrogen isopentane frozen diaphragm sections prepared for cryosectioning were cut at 10 µm, mounted on glass cover slips, and incubated overnight at 4℃ in antibody dilue nt (Dako, Hamburg, Germany) with primary antibodies against myosin heavy chain type I fibers (M8421, 1/400; Sigma, Taufkirchen, Germany) or laminin (1/200; Sigma, Taufkirchen, Germany). After washing with TBST, sections were incubated with fluorescently-conjugated (Alexa 488) secondary antibodies for 1 h, further washed, and then visualized under a fluorescent microscope. Images were captured at x5 magnification and merged to allow fiber morphology to be determined using imaging software (Analysis Five, Olympus, Münster, Germany), which included ~300-500 fibers in a muscle area of ~500,000 μm^2 (i.e., ~40-50% of the total muscle section). Stained fibers (bright green) were taken as type I, unstained fibers (black) as type II, with fiber boundaries demarcated in red. In addition, capillaries were stained with lectin specific to endothelial cells using rhodamine-conjugated Griffonia simplicifolia lectin-1 (1:250 dilution; Vector Laboratories Ltd, Peterborough, UK), with the capillary-to-fiber (C/F) ratio (number of capillaries to number of fibers) and capillary density (CD; number of capillaries per mm^2 of muscle tissue) calculated alongside the mean fiber cross sectional area (FCSA). Images were captured at x40 magnification, which included ~100 fibers in a muscle area of ~120,000 μm^2 (i.e., ~15% of the total muscle section).

Statistical analyses

Means were compared, where appropriate, with t-tests. Diaphragm muscle contractile function data were analyzed using a two-factor repeated measures ANOVA (contraction time × genotype and contraction frequency × genotype). Mitochondrial function data were analyzed using a two-factor repeated measures ANOVA (respiratory state × genotype). Data are presented as mean ± SD, and, where appropriate, the 95% confidence interval (CI_{95}) is included.

Results

In this conditional VEGF deficiency mouse model, we confirmed VEGF protein levels were lower in the diaphragm of SkmVEGF$^{-/-}$ mice compared to WT mice by ~50% (1.45±0.65 vs. 3.04±1.41 pg/total protein; P=0.001).

Contractile function

Specific force generated by diaphragm fiber bundles was impaired following VEGF deletion by ~15% in SkmVEGF$^{-/-}$ compared to WT mice (F[1,23] = 15.01, P=0.001; main effect of genotype), which occurred at both low and high stimulation frequencies ranging from 15 to 300 Hz (Fig 1A). Similarly, there was a rightward shift in the normalized force frequency relationship (F[1,23] = 2.98, P=0.045; interaction), with relative forces lower between 30 - 120 Hz in SkmVEGF$^{-/-}$ diaphragm fiber bundles (Fig. 1B). In contrast, fatigue resistance tended to be higher in SkmVEGF$^{-/-}$ compared to WT mice during the fatigue protocol (F[1,23] = 4.15, P=0.053; main effect of genotype), such that relative force tended to be ~10% higher throughout the repeated contractions (Fig. 1C). Twitch kinetics remained unaltered following VEGF deletion, with no differences (P>0.05) between WT and SkmVEGF$^{-/-}$ mice in terms of time to peak tension (TPT; 43±7 vs. 42±3 ms, respectively) and half-relaxation time (HRT; 60±17 vs. 63±16 ms, respectively).

Muscle structure and protein expression

The C/F ratio was ~40% lower in SkmVEGF$^{-/-}$ compared to WT mice (P=0.008; Fig. 2A). In contrast, the CD remained unchanged between groups (P>0.05; Fig. 2B) which can be explained by the scale-dependent consequence of VEGF deletion lowering mean FCSA in parallel (Fig. 2C; P=0.023). Representative muscle sections from WT and SkmVEGF$^{-/-}$ are presented in Fig. 2D-E. Fiber proportion for type I slow and type II fast myosin heavy chain isoforms were not different

between SkmVEGF$^{-/-}$ and WT mice (P=0.455; Fig. 2F), with type I fibers representing ~10 % of overall fiber population. In contrast, however, type I fiber cross-sectional area was lower by ~25 % in SkmVEGF$^{-/-}$ compared to WT mice (P=0.027; Fig. 2G). No difference was detected in type II fiber cross-sectional area between the groups (P=0.786; Fig. 2G). While no difference was observed between groups for MyHC expression (P=0.429; Fig. 3A), the smaller type I fiber size corresponded to an ~30% lower level of the key contractile protein actin (P=0.011; Fig. 3B). We subsequently measured key proteins known to be involved in fiber atrophy signaling, but found no differences between groups in relation to the key E3 ligase MAFBx (P=0.189; Fig. 4A) and major ROS source NADPH oxidase (P=0.091; Fig. 4B). We also probed for protein expression of key upstream regulatory proteins in the VEGF signaling cascade, but found no differences in protein expression of HIF-1α (P=0.417; Fig. 4C) and PGC-1α (P=0.176; Fig. 4D).

Mitochondrial function

Diaphragm mitochondrial O_2 consumption was not different between SkmVEGF$^{-/-}$ and WT (F[1,80] = 0.85, P=0.36, Fig 5A), nor was an interaction present (respiratory state × genotype: F[4,80] = 0.1, P=0.98, Fig 5A). However, H_2O_2 production was lower in SkmVEGF$^{-/-}$ vs WT (F[1,75] = 14.57, P=0.0003, Fig 5B), with particular differences observed at OXPHOS_CI+II and ETS_CII respiratory states. OXPHOS coupling efficiency, the ratio of free to total OXPHOS capacity, was not different between SkmVEGF$^{-/-}$ and WT (Fig 5C). There were no differences (P>0.05) in the flux control ratios (FCR) for ADP-stimulated respiration (Fig 5D-E) or in the substrate control ratio (SCR) for succinate (Fig 5F). Citrate synthase activity was also not different (P>0.05) between WT and SkmVEGF$^{-/-}$ mice (8.38±0.73 vs. 8.20±0.96 µmol/min/mg protein, respectively).

Discussion

We found that myofiber-specific VEGF deficient mice produce reduced specific tension in the diaphragm accompanied by a lower C/F ratio, fiber atrophy and loss of sarcomeric actin content. While the mechanisms linking VEGF signaling to diaphragm weakness remain unclear, we suggest it may be related to the lower number of capillaries supplying each fiber. This could limit oxygen and nutrient availability and affect contractile function via tissue hypoxia, inflammation, and/or protein homeostasis (23). Interestingly, diaphragmatic mitochondrial function and content were maintained in VEGF deficient mice and mitochondrial-derived ROS generation was lower. These findings suggest that vascular dysfunction may lead to metabolic compensation in myofibers that manifests as improved fatigue resistance measured in the absence of neural or vascular systems.

Myofiber-VEGF deletion leads to diaphragm weakness

Conditional gene deletion of skeletal myofiber-specific VEGF in adult mice reduced VEGF protein levels by ~50%. While other cells, including endothelial cells, macrophage stem cells and fibroblast express VEGF, myofibers are the major source of VEGF in skeletal muscle (50). Rather than life-long VEGF gene ablation, conditional deletion provides a more clinically relevant model to investigate whether diaphragm VEGF deficiency is linked to respiratory muscle weakness in adult patients. The reduction in diaphragm VEGF levels were similar to that reported previously in life-long skeletal myofiber targeted VEGF gene ablated (~60% reduction) 20 week old mice (50). Life-long VEGF deficiency reduces diaphragm capillarity by around 40%, and this reduction in capillaries was almost two-fold greater than that observed in locomotor muscles in this same mouse line (50). We observed a similar trend in the present study. Conditional VEGF gene-deletion induced in adult mice resulted in an ~40% lower C/F ratio in the diaphragm. However, in contrast to mice with life-long loss of the VEGF gene, locomotor skeletal muscle capillaries are stable when VEGF gene deletion is initiated in adult mice (16, 26).

While low VEGF levels are associated with conditions where diaphragm dysfunction is developed such as mechanical ventilation (11, 17), a direct link had not been previously explored. Given the diaphragm's high degree of sensitivity when homeostasis is challenged (6, 8, 9, 31, 32), we anticipated low VEGF expression would impair diaphragm contractile function. A major finding of our current study, therefore, was confirming that VEGF deficiency impairs isometric specific forces by ~15% in the diaphragm. These functional differences are similar to that observed in patients and experimental animal models where diaphragm fiber function is impaired, such as in mechanical ventilation, critical illness, and heart failure (24, 31, 40). The contractile dysfunction was present at both low (15-30 Hz) and high (120-300 Hz) stimulation frequencies, which indicates that low VEGF-dependent signaling could impact a range of respiratory movements, such as resting and exercising ventilation in addition to acute respiratory exacerbations involving airway clearance.

Our data add important knowledge to indicate that respiratory muscle shows a substantial degree of sensitivity to VEGF ablation. This is not surprising given the diaphragm shows a high sensitivity to dysfunction compared to the limbs when challenged by disease states such as heart failure (53), systemic hypertension (8), and pulmonary hypertension (14). Thus, the onset of diaphragm weakness may represent an early marker of disease. The mechanism(s) is likely underpinned by the diaphragm's persistent contraction pattern, which renders it highly susceptible to early changes in mechanical loading (possibly related to pulmonary/acid-base disturbance) and/or delivery of oxygen, nutrients, inflammatory cytokines, and ROS (23). Deficient skeletal myofiber VEGF levels are also linked to whole-body reductions in exercise tolerance (26, 50), and our data provide support that respiratory muscle weakness may be a contributing factor.

Mechanisms of VEGF-induced diaphragm weakness

The mechanism(s) by which VEGF deficiency induced diaphragm contractile dysfunction remains unclear. Our data confirmed impaired force generation at both low and high stimulation frequencies in isolated fiber bundles concomitant with a rightward shift in the normalized force-frequency relationship. Impaired forces at the low stimulation frequencies and the rightward shift in the normalized force-frequency relationship in VEGF deficient diaphragm fibers could be interpreted as a result of a slow-to-fast fiber type switch and/or alterations in calcium handling (i.e., more rapid Ca^{2+} release/reuptake dynamics). However, we found no changes between groups in terms of fiber type or twitch kinetics, which would argue against such mechanisms acting. However, we did find that protein expression of sarcomeric actin was ~25% lower in the diaphragm of SkmVEGF$^{-/-}$ mice, which could directly limit cross-bridge cycling thus limiting force generating capacity. It remains unclear why we observed a preferential loss of actin compared to myosin. A disproportionate loss between the major contractile proteins is not uncommon and this has been reported in various conditions including critical illness myopathy, immobilization, and microgravity (21, 35). Under conditions of VEGF deficiency, therefore, various mechanisms may be induced in the diaphragm including the preferential degradation of actin (following specific targeting of numerous activated E3 ligases), impaired transcription and synthesis of actin, and/or an imbalance in protein turnover rates between actin and myosin (21, 35).

The lower actin content was also a likely factor underlying atrophy preferentially observed in type I fibers in the diaphragm of SkmVEGF$^{-/-}$ mice. The reason for why we observed a preferential fiber type I atrophy in VEGF deficient skeletal muscle remains unclear, but it may be consequent to type I fibers having a more rich capillary supply than type II fibers. Therefore, type I fibers may be more susceptible to contractile protein loss (and thus atrophy) under conditions associated with VEGF deficiency that severely impair capillary maintenance [e.g., cigarette smoke exposure; (34, 52)]. Interestingly, loss of thin filaments may increase the maximal shortening velocity (V_{max}) even

without a change in MyHC (42). Without a measure of V_{max}, however, we can only speculate at this point.

It is important to note that it remains unclear how much this loss of actin actually contributed to the observed contractile weakness/type I fiber atrophy given the small proportion of type I fibers present in mouse diaphragm. Nonetheless, in other diseases where O_2 delivery is impaired, such as heart failure and COPD, reduced actin content in combination with muscle dysfunction and atrophy are present (7, 30, 47). In muscle wasting following dexamethasone treatment or cigarette exposure in mice, VEGF protein expression is also reduced (4). In combination, these findings suggest VEGF may play a critical role in modulating protein homeostasis. However, we wish to note a few limitations in our methodology, which include not distinguishing between the type II fiber subtypes (a, x, b) and use of a low salt buffer to assess levels of MyHC and actin where total abundance may not be accurately reflected if incompletely solubilized (43).

The signaling pathways responsible for protein loss and fiber atrophy in VEGF deficiency remain unclear, but likely include an upregulation in protein degradation and/or a downregulation in protein synthesis in muscle with insufficient supply of O_2. Given that conditional VEGF ablation led to around a ~40% lower C/F ratio and as previous data have shown it can also impair muscle perfusion (26, 50), it is possible that VEGF deficiency in muscle induces tissue hypoxia to activate proteolytic pathways (15). It is important to note that this is speculative, as we do not have a measure of diaphragm tissue hypoxia in vivo from the current study. Nonetheless, as protein levels of the key E3 ligase atrogene MAFbx were not different between WT and SkmVEGF$^{-/-}$ mice suggests diaphragm VEGF deficiency may upregulate other key atrophic pathways associated with contractile protein degradation (e.g., calpain, caspase-3, MuRF1, or increased ubiquitin proteasome activity; (7, 30, 48)) or via inhibition of protein synthesis (e.g., Akt, mTOR, p70S6K

(45)). Future investigation into the role VEGF exerts over various protein synthesis/degradation signaling molecules may therefore prove worthwhile.

Elevated ROS in the diaphragm in disease can also stimulate protein degradation (45) and induce post-translational oxidative contractile protein modifications (9). However, as our ROS measures of mitochondrial as well as transmembrane NADPH oxidase were not elevated in SkmVEGF$^{-/-}$, with both known to be strong mediators of diaphragm weakness (1), this argues against VEGF deficiency inducing diaphragm weakness via a ROS-related mechanism. However, an activity-based assay of NADPH oxidase should be considered for future experiments. We also probed upstream regulators involved in the VEGF signaling cascade for potential compensatory adaptations to the VEGF deficiency. Both HIF-1α and PGC-1α independently stimulate VEGF (3), with VEGF generally secreted by the transcription factor HIF-1α in response to hypoxic conditions (19) and by the transcriptional coactivator PGC-1α in response to exercise (29). Both HIF-1α and PGC-1α signaling in diaphragm tissue were not impacted in the present study indicating they do not form part of a compensatory response to VEGF deficiency.

VEGF deletion does not impact diaphragm mitochondrial respiration

Mitochondrial impairments are developed in diseases associated with diaphragm dysfunction (38, 40). However, in our study in situ mitochondrial O_2 consumption was not impacted. Neither mitochondrial content (as assessed by citrate synthase) nor the coupling efficiency or respiratory capacity were different under VEGF deficiency. Whether the fiber atrophy that occurred following VEGF deficiency acted as a compensatory mechanism to maintain mitochondrial respiratory function remains unclear but seems a reasonable suggestion. For example, in response to derangements in muscle perfusion, a lower muscle size may help maintain adequate O_2 diffusion between capillary and myocyte (26).

In contrast, mitochondrial-derived ROS flux was lower following VEGF ablation. The mechanisms underlying lower mitochondrial ROS flux in SkmVEGF$^{-/-}$ mice remains uncertain, but it could be related to a higher anti-oxidant enzyme capacity. For example, a compensatory increase in oxidative enzyme activity (i.e., citrate synthase, β-HAD) occurs in both locomotor and diaphragm muscle in mice with VEGF deficiency from birth (36) and in the gastrocnemius following conditional deletion (16). As a shift towards greater muscle oxidative capacity is commonly associated with increased anti-oxidant enzyme activities (e.g., superoxide dismutase, glutathione peroxidase, catalase) (39), this could be a plausible explanation for why mitochondrial ROS flux may be lower. However our current data showed citrate synthase activity remained unchanged.

High mitochondrial ROS production is particularly common in conditions associated with diaphragm weakness, such as heart failure (28) and mechanical ventilation (40). Surprisingly, we found that mitochondrial-derived ROS flux was lower in VEGF deficient diaphragm fibers. As NADPH oxidase, a cytosolic ROS marker, was also not different between groups, our data indicate that diaphragm weakness induced by VEGF deficiency is unlikely to be mediated by elevated oxidative stress. SkmVEGF$^{-/-}$ mice may have been better protected against ROS-induced muscle fatigue, as increased ROS production during repeated contractions inhibits force generation (12). Interestingly, improvements in relative fatigue of the diaphragm in vitro are also present in disease (31), which suggests the SkmVEGF$^{-/-}$ mouse model may closely reflect pathological states and thus mirror adaptations to that often observed after long-term endurance training (39). However, the observation of this improved fatigue resistance may be dependent on the in vitro muscle fatigue protocol employed. Using a “matched-stimulus” rather than “matched-initial specific force” protocol, healthy (or control) diaphragm fibers generate higher absolute forces initially and throughout to induce an apparent more rapid fatigue (20, 31). Therefore, the fatigue protocol employed in our study may explain why relative fatigue resistance was higher in mice with VEGF deficiency and extrapolation of these findings should be interpreted with caution.

Conclusions

Skeletal myofiber-specific VEGF deletion resulted in diaphragm contractile dysfunction that was accompanied by lower CF ratio, smaller type I fibers, lower sarcomeric actin protein, and lower mitochondrial ROS generation. Whether differences in type I fiber size, capillarity, and ROS generation compensated to protect mitochondrial respiratory function remains unclear. Deficient diaphragm VEGF levels may be a contributing factor to the onset of diaphragm dysfunction and provide a viable treatment target for patients afflicted with respiratory muscle weakness.

Competing Interests

Authors have no competing interests.

Funding

NIH/NLBI1 P01 HL091830-01A1

TRDRP 26IP-0033

TSB acknowledges support from the Fondation Leducq (TNE 13CVD04) and the Medical Research Council UK (MR/S025472/1).

Acknowledgements

We thank Professor Mike Hogan from the UCSD for his kind assistance with the muscle function measurements, Dr. Roger Kissane from the University of Leeds for his kind advice regarding capillary staining, Angela Kricke from Leipzig Heart Center for technical support, Professor Napoleone Ferrara and Genentech for kindly allowing us to use the VEGFLoxP mice, and Drs. Daniel Metzger and Pierre Chambon from the Institut de Génétique et de Biologie Moléculaire et Cellulaire for generously providing the HSA-CreER^{T2} mouse strain.

References

1. **Ahn B, Beharry AW, Frye GS, Judge AR, and Ferreira LF**. NAD(P)H oxidase subunit p47phox is elevated, and p47phox knockout prevents diaphragm contractile dysfunction in heart failure. Am J Physiol Lung Cell Mol Physiol 309: L497-505, 2015.

2. **Alexopoulou C, Mitrouska I, Arvanitis D, Tzanakis N, Chalkiadakis G, Melissas J, Zervou M, and Siafakas N**. Vascular-specific growth factor mRNA levels in the human diaphragm. Respiration 72: 636-641, 2005.

3. **Arany Z, Foo SY, Ma Y, Ruas JL, Bommi-Reddy A, Girnun G, Cooper M, Laznik D, Chinsomboon J, Rangwala SM, Baek KH, Rosenzweig A, and Spiegelman BM**. HIF-independent regulation of VEGF and angiogenesis by the transcriptional coactivator PGC-1alpha. Nature 451: 1008-1012, 2008.

4. **Barel M, Perez OA, Giozzet VA, Rafacho A, Bosqueiro JR, and do Amaral SL**. Exercise training prevents hyperinsulinemia, muscular glycogen loss and muscle atrophy induced by dexamethasone treatment. Eur J Appl Physiol 108: 999-1007, 2010.

5. **Barreiro E, Schols AM, Polkey MI, Galdiz JB, Gosker HR, Swallow EB, Coronell C, Gea J, and project EiC**. Cytokine profile in quadriceps muscles of patients with severe COPD. Thorax 63: 100-107, 2008.

6. **Bowen TS, Aakeroy L, Eisenkolb S, Kunth P, Bakkerud F, Wohlwend M, Ormbostad AM, Fischer T, Wisloff U, Schuler G, Steinshamn S, Adams V, and Bronstad E**. Exercise Training Reverses Extrapulmonary Impairments in Smoke-exposed Mice. Medicine and science in sports and exercise 49: 879-887, 2017.

7. **Bowen TS, Adams V, Werner S, Fischer T, Vinke P, Brogger MN, Mangner N, Linke A, Sehr P, Lewis J, Labeit D, Gasch A, and Labeit S**. Small-molecule inhibition of MuRF1 attenuates skeletal muscle atrophy and dysfunction in cardiac cachexia. Journal of cachexia, sarcopenia and muscle 8: 939-953, 2017.

8. **Bowen TS, Eisenkolb S, Drobner J, Fischer T, Werner S, Linke A, Mangner N, Schuler G, and Adams V**. High-intensity interval training prevents oxidant-mediated diaphragm muscle weakness in hypertensive mice. FASEB journal : official publication of the Federation of American Societies for Experimental Biology 31: 60-71, 2017.

9. **Bowen TS, Mangner N, Werner S, Glaser S, Kullnick Y, Schrepper A, Doenst T, Oberbach A, Linke A, Steil L, Schuler G, and Adams V**. Diaphragm muscle weakness in mice is early-onset post-myocardial infarction and associated with elevated protein oxidation. J Appl Physiol (1985) 118: 11-19, 2015.

10. **Breen EC**. VEGF in biological control. Journal of cellular biochemistry 102: 1358-1367, 2007.

11. **Bruells CS, Maes K, Rossaint R, Thomas D, Cielen N, Bleilevens C, Bergs I, Loetscher U, Dreier A, Gayan-Ramirez G, Behnke BJ, and Weis J**. Prolonged

mechanical ventilation alters the expression pattern of angio-neogenetic factors in a pre-clinical rat model. PLoS One 8: e70524, 2013.

12. **Cheng AJ, Yamada T, Rassier DE, Andersson DC, Westerblad H, and Lanner JT**. Reactive oxygen/nitrogen species and contractile function in skeletal muscle during fatigue and recovery. The Journal of physiology 594: 5149-5160, 2016.

13. **Close RI**. Dynamic properties of mammalian skeletal muscles. Physiol Rev 52: 129-197, 1972.

14. **de Man FS, van Hees HW, Handoko ML, Niessen HW, Schalij I, Humbert M, Dorfmuller P, Mercier O, Bogaard HJ, Postmus PE, Westerhof N, Stienen GJ, van der Laarse WJ, Vonk-Noordegraaf A, and Ottenheijm CA**. Diaphragm muscle fiber weakness in pulmonary hypertension. Am J Respir Crit Care Med 183: 1411-1418, 2011.

15. **de Theije CC, Langen RC, Lamers WH, Schols AM, and Kohler SE**. Distinct responses of protein turnover regulatory pathways in hypoxia- and semistarvation-induced muscle atrophy. Am J Physiol Lung Cell Mol Physiol 305: L82-91, 2013.

16. **Delavar H, Nogueira L, Wagner PD, Hogan MC, Metzger D, and Breen EC**. Skeletal myofiber VEGF is essential for the exercise training response in adult mice. American journal of physiology Regulatory, integrative and comparative physiology 306: R586-595, 2014.

17. **DeRuisseau KC, Shanely RA, Akunuri N, Hamilton MT, Van Gammeren D, Zergeroglu AM, McKenzie M, and Powers SK**. Diaphragm unloading via controlled mechanical ventilation alters the gene expression profile. Am J Respir Crit Care Med 172: 1267-1275, 2005.

18. **Dres M, Dube BP, Mayaux J, Delemazure J, Reuter D, Brochard L, Similowski T, and Demoule A**. Coexistence and Impact of Limb Muscle and Diaphragm Weakness at Time of Liberation from Mechanical Ventilation in Medical Intensive Care Unit Patients. Am J Respir Crit Care Med 195: 57-66, 2017.

19. **Ferrara N, Gerber HP, and LeCouter J**. The biology of VEGF and its receptors. Nat Med 9: 669-676, 2003.

20. **Ferreira LF, Moylan JS, Gilliam LA, Smith JD, Nikolova-Karakashian M, and Reid MB**. Sphingomyelinase stimulates oxidant signaling to weaken skeletal muscle and promote fatigue. Am J Physiol Cell Physiol 299: C552-560, 2010.

21. **Fitts RH, Riley DR, and Widrick JJ**. Physiology of a microgravity environment invited review: microgravity and skeletal muscle. J Appl Physiol (1985) 89: 823-839, 2000.

22. **Gerber HP, Hillan KJ, Ryan AM, Kowalski J, Keller GA, Rangell L, Wright BD, Radtke F, Aguet M, and Ferrara N**. VEGF is required for growth and survival in neonatal mice. Development 126: 1149-1159, 1999.

23. **Greising SM, Ottenheijm CAC, O'Halloran KD, and Barreiro E**. Diaphragm plasticity in aging and disease: therapies for muscle weakness go from strength to strength. J Appl Physiol (1985) 125: 243-253, 2018.

24. **Hooijman PE, Beishuizen A, Witt CC, de Waard MC, Girbes AR, Spoelstra-de Man AM, Niessen HW, Manders E, van Hees HW, van den Brom CE, Silderhuis V, Lawlor MW, Labeit S, Stienen GJ, Hartemink KJ, Paul MA, Heunks LM, and Ottenheijm CA**. Diaphragm muscle fiber weakness and ubiquitin-proteasome activation in critically ill patients. Am J Respir Crit Care Med 191: 1126-1138, 2015.

25. **Huey KA, Smith SA, Sulaeman A, and Breen EC**. Skeletal myofiber VEGF is necessary for myogenic and contractile adaptations to functional overload of the plantaris in adult mice. J Appl Physiol (1985) 120: 188-195, 2016.

26. **Knapp AE, Goldberg D, Delavar H, Trisko BM, Tang K, Hogan MC, Wagner PD, and Breen EC**. Skeletal myofiber VEGF regulates contraction-induced perfusion and exercise capacity but not muscle capillarity in adult mice. American journal of physiology Regulatory, integrative and comparative physiology 311: R192-199, 2016.

27. **Krumschnabel G, Fontana-Ayoub M, Sumbalova Z, Heidler J, Gauper K, Fasching M, and Gnaiger E**. Simultaneous high-resolution measurement of mitochondrial respiration and hydrogen peroxide production. Methods Mol Biol 1264: 245-261, 2015.

28. **Laitano O, Ahn B, Patel N, Coblentz PD, Smuder AJ, Yoo JK, Christou DD, Adhihetty PJ, and Ferreira LF**. Pharmacological targeting of mitochondrial reactive oxygen species counteracts diaphragm weakness in chronic heart failure. J Appl Physiol (1985) 120: 733-742, 2016.

29. **Leick L, Hellsten Y, Fentz J, Lyngby SS, Wojtaszewski JF, Hidalgo J, and Pilegaard H**. PGC-1alpha mediates exercise-induced skeletal muscle VEGF expression in mice. Am J Physiol Endocrinol Metab 297: E92-103, 2009.

30. **Levine S, Biswas C, Dierov J, Barsotti R, Shrager JB, Nguyen T, Sonnad S, Kucharchzuk JC, Kaiser LR, Singhal S, and Budak MT**. Increased proteolysis, myosin depletion, and atrophic AKT-FOXO signaling in human diaphragm disuse. Am J Respir Crit Care Med 183: 483-490, 2011.

31. **Mangner N, Bowen TS, Werner S, Fischer T, Kullnick Y, Oberbach A, Linke A, Steil L, Schuler G, and Adams V**. Exercise Training Prevents Diaphragm Contractile Dysfunction in Heart Failure. Medicine and science in sports and exercise 48: 2118-2124, 2016.

32. **Mangner N, Weikert B, Bowen TS, Sandri M, Hollriegel R, Erbs S, Hambrecht R, Schuler G, Linke A, Gielen S, and Adams V**. Skeletal muscle alterations in chronic heart failure: differential effects on quadriceps and diaphragm. Journal of cachexia, sarcopenia and muscle 6: 381-390, 2015.

33. **Meyer FJ, Borst MM, Zugck C, Kirschke A, Schellberg D, Kubler W, and Haass M**. Respiratory muscle dysfunction in congestive heart failure: clinical correlation and prognostic significance. Circulation 103: 2153-2158, 2001.

34. **Nogueira L, Trisko BM, Lima-Rosa FL, Jackson J, Lund-Palau H, Yamaguchi M, and Breen EC**. Cigarette smoke directly impairs skeletal muscle function through capillary regression and altered myofibre calcium kinetics in mice. The Journal of physiology 596: 2901-2916, 2018.

35. **Ochala J, Gustafson AM, Diez ML, Renaud G, Li M, Aare S, Qaisar R, Banduseela VC, Hedstrom Y, Tang X, Dworkin B, Ford GC, Nair KS, Perera S, Gautel M, and Larsson L**. Preferential skeletal muscle myosin loss in response to mechanical silencing in a novel rat intensive care unit model: underlying mechanisms. The Journal of physiology 589: 2007-2026, 2011.

36. **Olfert IM, Howlett RA, Tang K, Dalton ND, Gu Y, Peterson KL, Wagner PD, and Breen EC**. Muscle-specific VEGF deficiency greatly reduces exercise endurance in mice. The Journal of physiology 587: 1755-1767, 2009.

37. **Pesta D, and Gnaiger E**. High-resolution respirometry: OXPHOS protocols for human cells and permeabilized fibers from small biopsies of human muscle. Methods Mol Biol 810: 25-58, 2012.

38. **Picard M, Jung B, Liang F, Azuelos I, Hussain S, Goldberg P, Godin R, Danialou G, Chaturvedi R, Rygiel K, Matecki S, Jaber S, Des Rosiers C, Karpati G, Ferri L, Burelle Y, Turnbull DM, Taivassalo T, and Petrof BJ**. Mitochondrial dysfunction and lipid accumulation in the human diaphragm during mechanical ventilation. Am J Respir Crit Care Med 186: 1140-1149, 2012.

39. **Powers SK, Criswell D, Lawler J, Martin D, Ji LL, Herb RA, and Dudley G**. Regional training-induced alterations in diaphragmatic oxidative and antioxidant enzymes. Respir Physiol 95: 227-237, 1994.

40. **Powers SK, Hudson MB, Nelson WB, Talbert EE, Min K, Szeto HH, Kavazis AN, and Smuder AJ**. Mitochondria-targeted antioxidants protect against mechanical ventilation-induced diaphragm weakness. Crit Care Med 39: 1749-1759, 2011.

41. **Powers SK, Wiggs MP, Sollanek KJ, and Smuder AJ**. Ventilator-induced diaphragm dysfunction: cause and effect. American journal of physiology Regulatory, integrative and comparative physiology 305: R464-477, 2013.

42. **Riley DA, Bain JL, Thompson JL, Fitts RH, Widrick JJ, Trappe SW, Trappe TA, and Costill DL**. Disproportionate loss of thin filaments in human soleus muscle after 17-day bed rest. Muscle Nerve 21: 1280-1289, 1998.

43. **Roberts BM, Ahn B, Smuder AJ, Al-Rajhi M, Gill LC, Beharry AW, Powers SK, Fuller DD, Ferreira LF, and Judge AR**. Diaphragm and ventilatory dysfunction during

cancer cachexia. FASEB journal : official publication of the Federation of American Societies for Experimental Biology 27: 2600-2610, 2013.

44. **Schuler M, Ali F, Metzger E, Chambon P, and Metzger D**. Temporally controlled targeted somatic mutagenesis in skeletal muscles of the mouse. Genesis 41: 165-170, 2005.

45. **Shanely RA, Van Gammeren D, Deruisseau KC, Zergeroglu AM, McKenzie MJ, Yarasheski KE, and Powers SK**. Mechanical ventilation depresses protein synthesis in the rat diaphragm. Am J Respir Crit Care Med 170: 994-999, 2004.

46. **Siafakas NM, Jordan M, Wagner H, Breen EC, Benoit H, and Wagner PD**. Diaphragmatic angiogenic growth factor mRNA responses to increased ventilation caused by hypoxia and hypercapnia. Eur Respir J 17: 681-687, 2001.

47. **Simonini A, Massie BM, Long CS, Qi M, and Samarel AM**. Alterations in skeletal muscle gene expression in the rat with chronic congestive heart failure. J Mol Cell Cardiol 28: 1683-1691, 1996.

48. **Supinski GS, Wang W, and Callahan LA**. Caspase and calpain activation both contribute to sepsis-induced diaphragmatic weakness. J Appl Physiol (1985) 107: 1389-1396, 2009.

49. **Taimeh Z, Loughran J, Birks EJ, and Bolli R**. Vascular endothelial growth factor in heart failure. Nat Rev Cardiol 10: 519-530, 2013.

50. **Tang K, Gu Y, Dalton ND, Wagner H, Peterson KL, Wagner PD, and Breen EC**. Selective Life-Long Skeletal Myofiber-Targeted VEGF Gene Ablation Impairs Exercise Capacity in Adult Mice. Journal of cellular physiology 231: 505-511, 2016.

51. **Tang K, Rossiter HB, Wagner PD, and Breen EC**. Lung-targeted VEGF inactivation leads to an emphysema phenotype in mice. J Appl Physiol 97: 1559-1566; discussion 1549, 2004.

52. **Tang K, Wagner PD, and Breen EC**. TNF-alpha-mediated reduction in PGC-1alpha may impair skeletal muscle function after cigarette smoke exposure. Journal of cellular physiology 222: 320-327, 2010.

53. **van Hees HW, Ottenheijm CA, Granzier HL, Dekhuijzen PN, and Heunks LM**. Heart failure decreases passive tension generation of rat diaphragm fibers. Int J Cardiol 141: 275-283, 2010.

Figure Legends

Figure 1. Diaphragm contractile function in skeletal muscle-specific VEGF deficient (skmVEGF$^{-/-}$) mice compared to wild type (WT) controls. Isolated diaphragm fiber bundles were stimulated at increasing stimulation frequencies to measure isometric specific force (**A**) and normalized relative to maximum force **(B),** with fatigability assessed during repeated stimulations (**C**). Data are mean±SD. *P<0.01; §P<0.05 skmVEGF$^{-/-}$ vs WT.

Figure 2. Diaphragm structural properties in skeletal muscle specific-VEGF deficient (skmVEGF$^{-/-}$) mice compared to wild type (WT) controls, which included assessment of capillary-to-fiber (C/F) ratio **(A)**, capillary density (CD) **(B)**, and mean fiber cross-sectional area (FCSA) **(C)** (n = 5 per group). Representative immunofluorescent diaphragm sections from WT (**D**) and skmVEGF$^{-/-}$ (**E**) mice (fiber boundaries stained red, type I fibers green, and type II fibers unstained), revealed no change in fiber type proportions (**F**) but a type I specific fiber atrophy in skmVEGF$^{-/-}$ mice compared to WT controls (n = 8-11 per group). Data are presented as mean±SD. *P<0.05 skmVEGF$^{-/-}$ vs WT.

Figure 3. Protein expression in the diaphragm of the key contractile proteins myosin heavy chain (MyHC; **A**) and sarcomeric actin (**B**), as well as respective representative blots (**C**) in skeletal muscle-specific VEGF deficient (skmVEGF$^{-/-}$) mice compared to wild type (WT) controls. Data were normalized to the loading control GAPDH and calculated as fold change (∆) vs. WT. Data are presented as mean±SD. *P=0.01 skmVEGF$^{-/-}$ vs WT.

Figure 4. Diaphragm protein expression along with representative blots of regulatory muscle signalling proteins measured in skeletal muscle-specific VEGF deficient (skmVEGF$^{-/-}$) mice compared to wild type (WT) controls, which included the key atrogin MAFBx (**A**) and ROS source NADPH oxidase (subunit gp91^{phox}) (**B**), as well as the upstream VEGF activators HIF-1α (**C**) and

PGC-1α (**D**). Data were normalized to the loading control GAPDH and calculated as fold change (Δ) vs. WT. Data are presented as mean±SD.

Figure 5. Diaphragm mitochondrial respiratory function and ROS production. Rate of oxygen consumption (JO_2) measured during a high-resolution respirometry substrate-uncoupler-inhibitor-titration (SUIT) protocol. **Panel A:** LEAK: glutamate+malate for LEAK state respiration. OXPHOS_CI: ADP for the phosphorylating state with substrates provided to complex I. OXPHOS_CI+II: ADP+succinate. ETS: Carbonyl cyanide m-chlorophenyl hydrazine for uncoupled respiration and electron transport system capacity. ETS_CII: Rotenone added to inhibit complex I. **Panel B:** H_2O_2 flux measured simultaneous to JO_2. Main effect of genotype present ($F[1, 75] = 14.57$, $P=0.0003$) and * denotes different to WT. **Panel C:** OXPHOS coupling efficiency was calculated as (1-LEAK / OXPHOS_CI+II). **Panel D:** Flux control ratio (FCR) for OXPHOS_CI was calculated as (OXPHOS_CI / ETS). **Panel E:** FCR for OXPHOS_CI+II was calculated as (OXPHOS_CI+II / ETS). **Panel F:** Substrate control ratio (SCR) for succinate was calculated as (OXPHOS_CI+II / OXPHOS_CI). Error bars are SD, n=8-10.

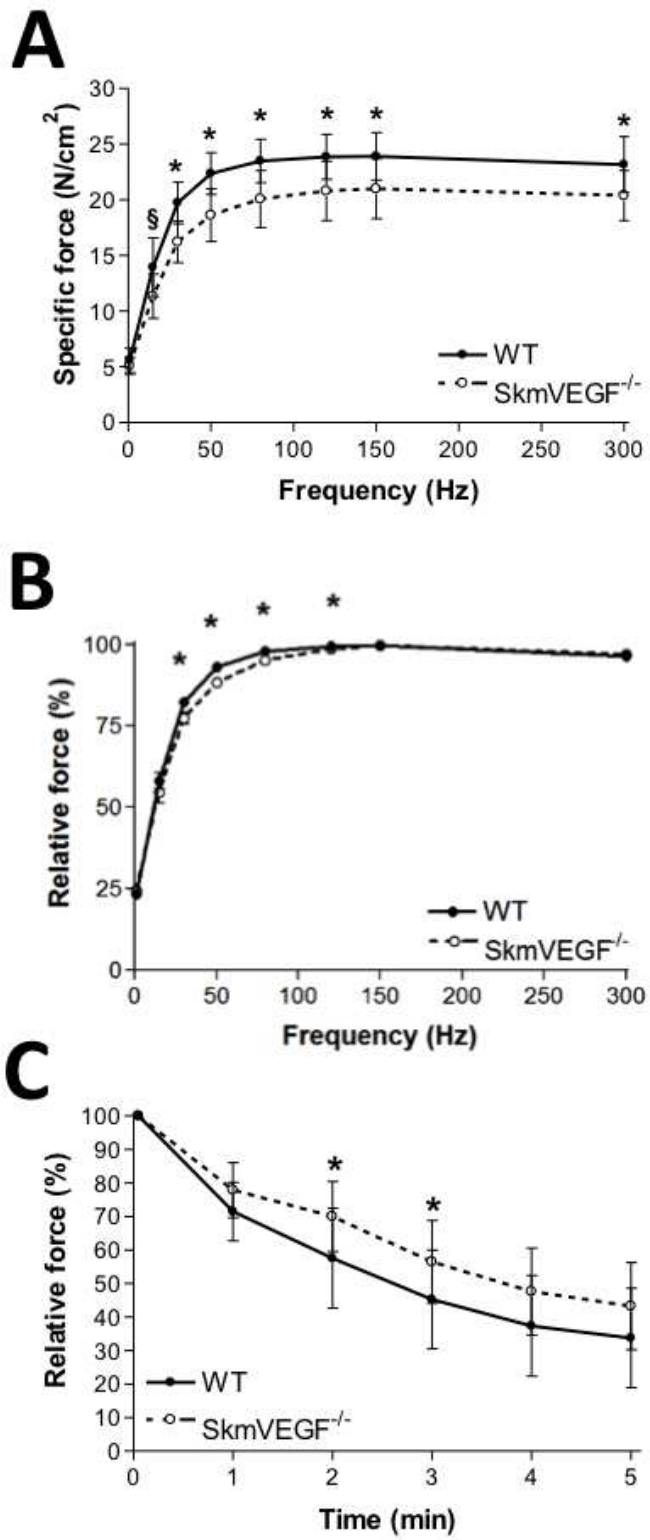
A
Specific force (N/cm2)
Frequency (Hz)
WT
SkmVEGF-/-
B
Relative force (%)
Frequency (Hz)
WT
SkmVEGF-/-
C
Relative force (%)
Time (min)
WT
SkmVEGF-/-

Figure 1.

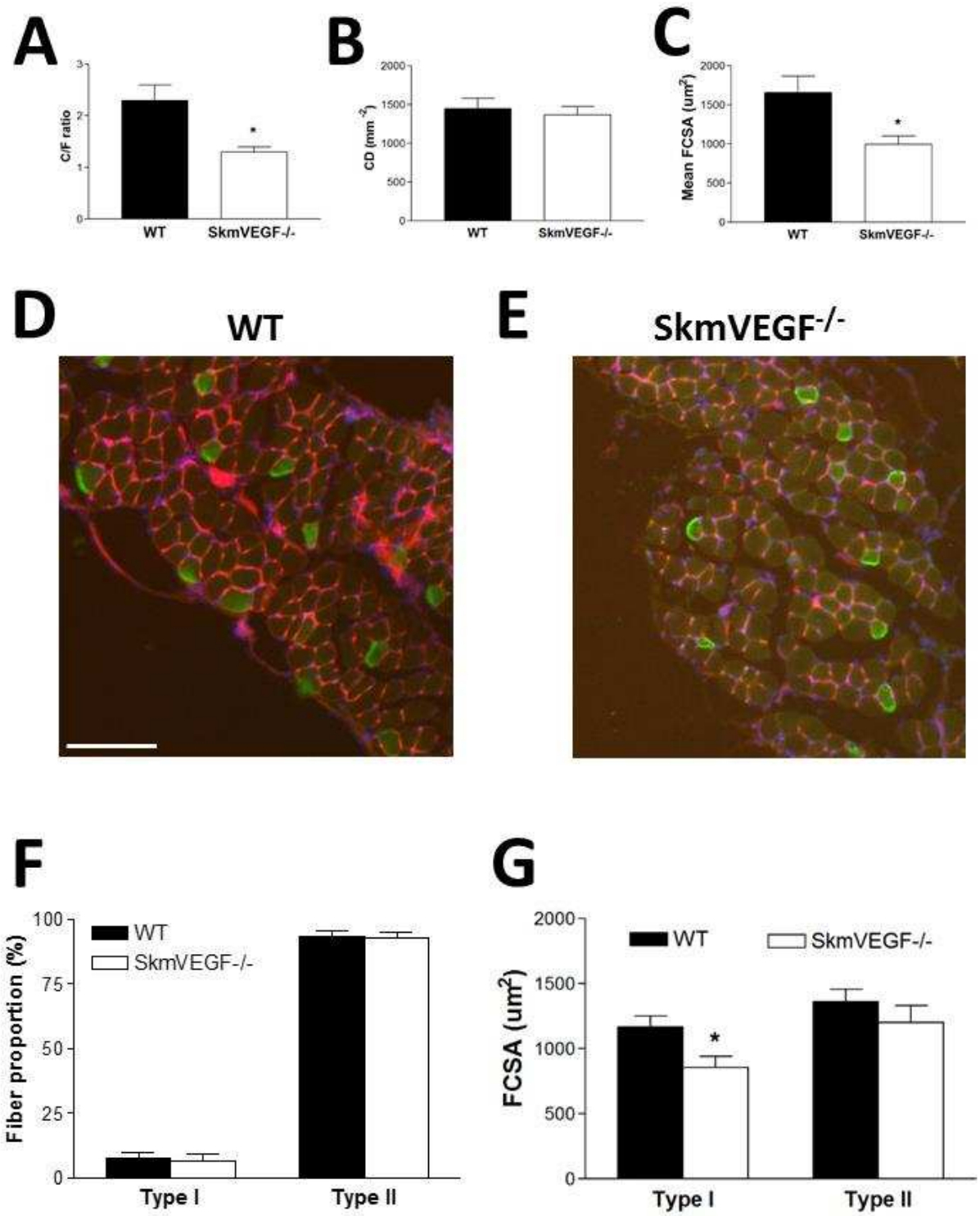
A
C/F ratio
WT
SkmVEGF-/-
B
CD (mm -2)
WT
SkmVEGF-/-
C
Mean FCSA (um2)
WT
SkmVEGF-/-
D
WT
E
SkmVEGF-/-
F
Fiber proportion (%)
WT
SkmVEGF-/-
Type I
Type II
G
FCSA (um2)
WT
SkmVEGF-/-
Type I
Type II

Figure 2.

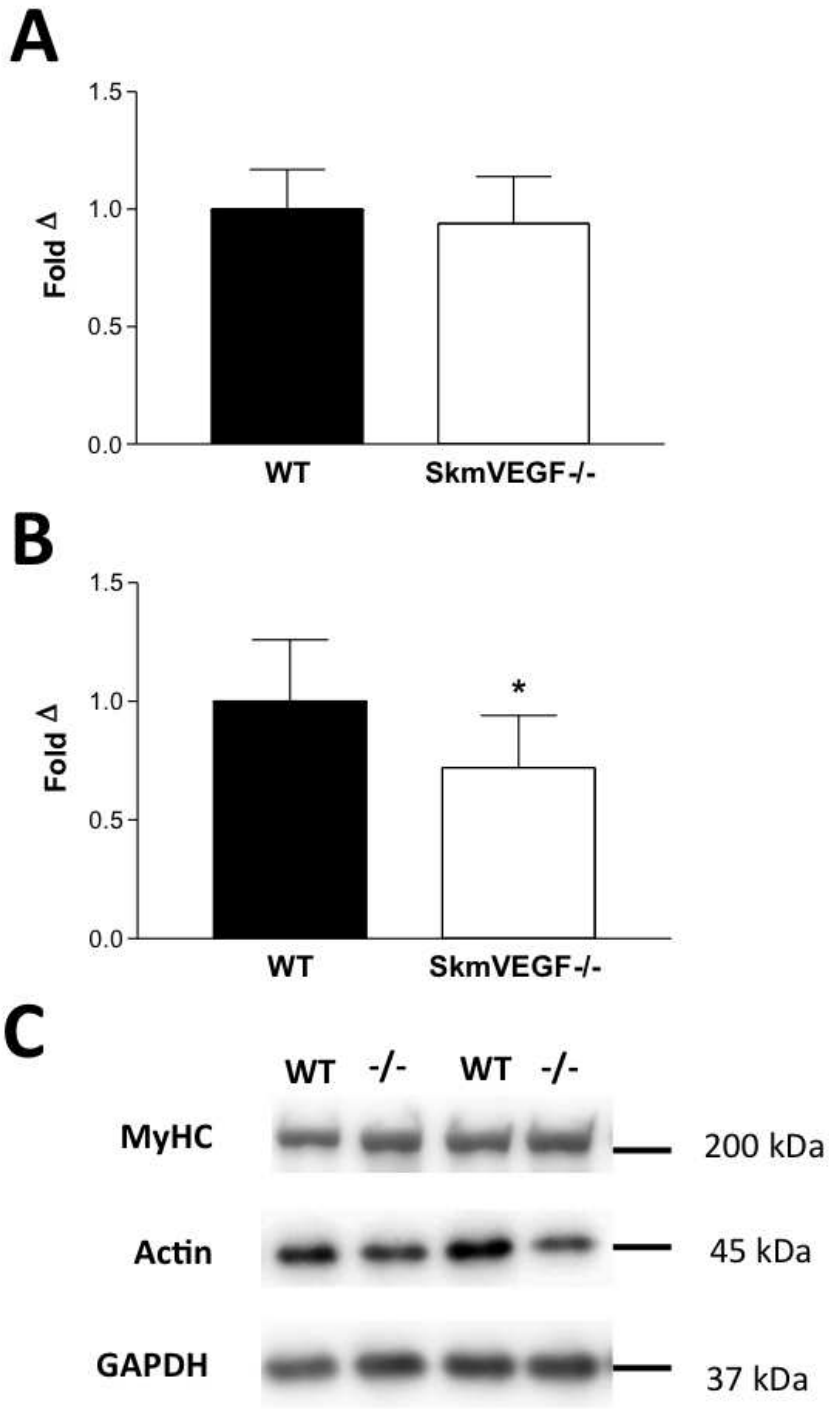
A
1.5
1.0
0.5
0.0
Fold Δ
WT
SkmVEGF-/-
B
1.5
1.0
0.5
0.0
Fold Δ
*
WT
SkmVEGF-/-
C
WT
-/-
WT
-/-
MyHC
200 kDa
Actin
45 kDa
GAPDH
37 kDa

Figure 3.

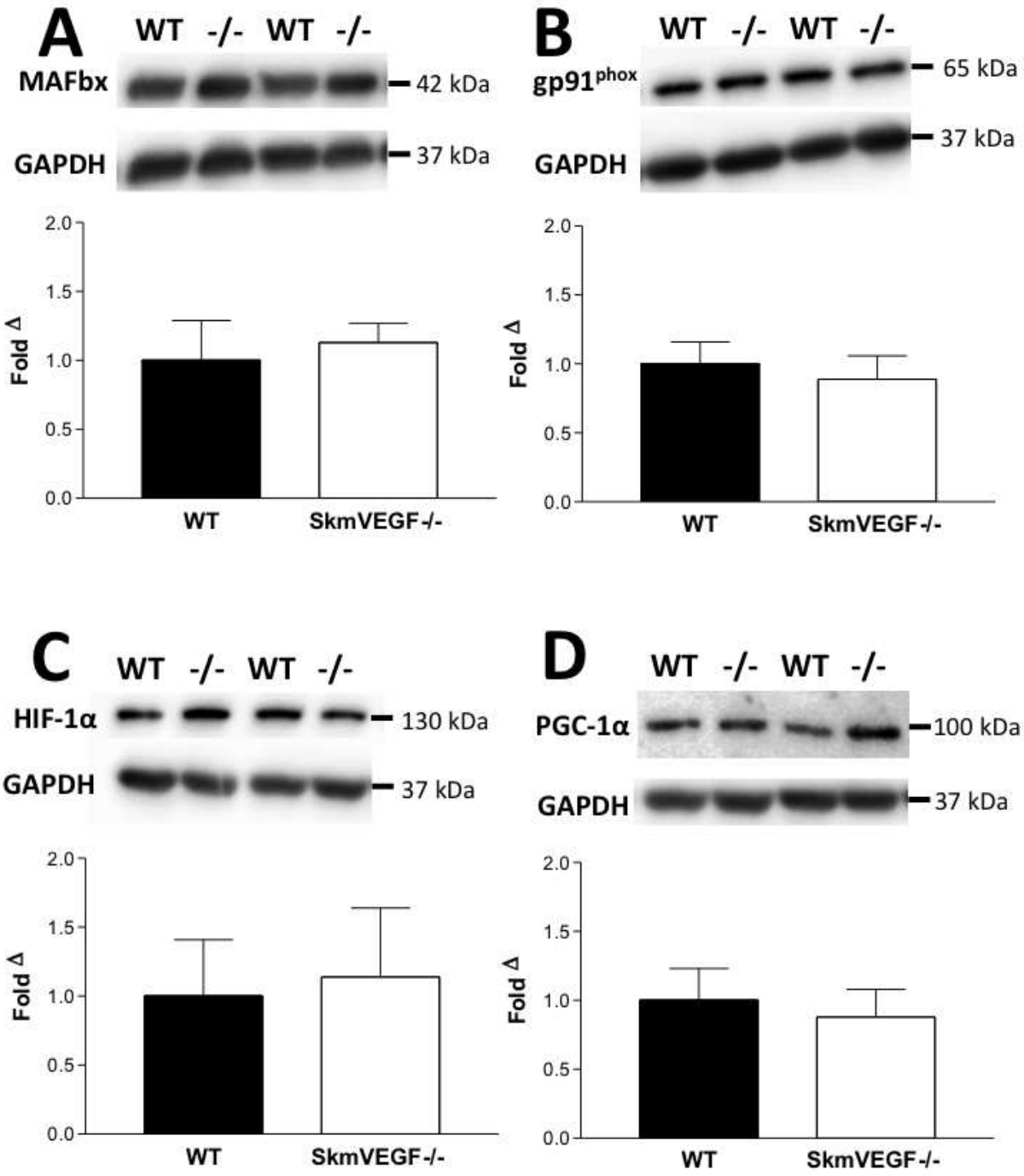
A
WT -/- WT -/-
MAFbx
42 kDa
GAPDH
37 kDa
Fold Δ
2.0
1.5
1.0
0.5
0.0
WT
SkmVEGF-/-
B
WT -/- WT -/-
gp91phox
65 kDa
GAPDH
37 kDa
Fold Δ
2.0
1.5
1.0
0.5
0.0
WT
SkmVEGF-/-
C
WT -/- WT -/-
HIF-1α
130 kDa
GAPDH
37 kDa
Fold Δ
2.0
1.5
1.0
0.5
0.0
WT
SkmVEGF-/-
D
WT -/- WT -/-
PGC-1α
100 kDa
GAPDH
37 kDa
Fold Δ
2.0
1.5
1.0
0.5
0.0
WT
SkmVEGF-/-

Figure 4.

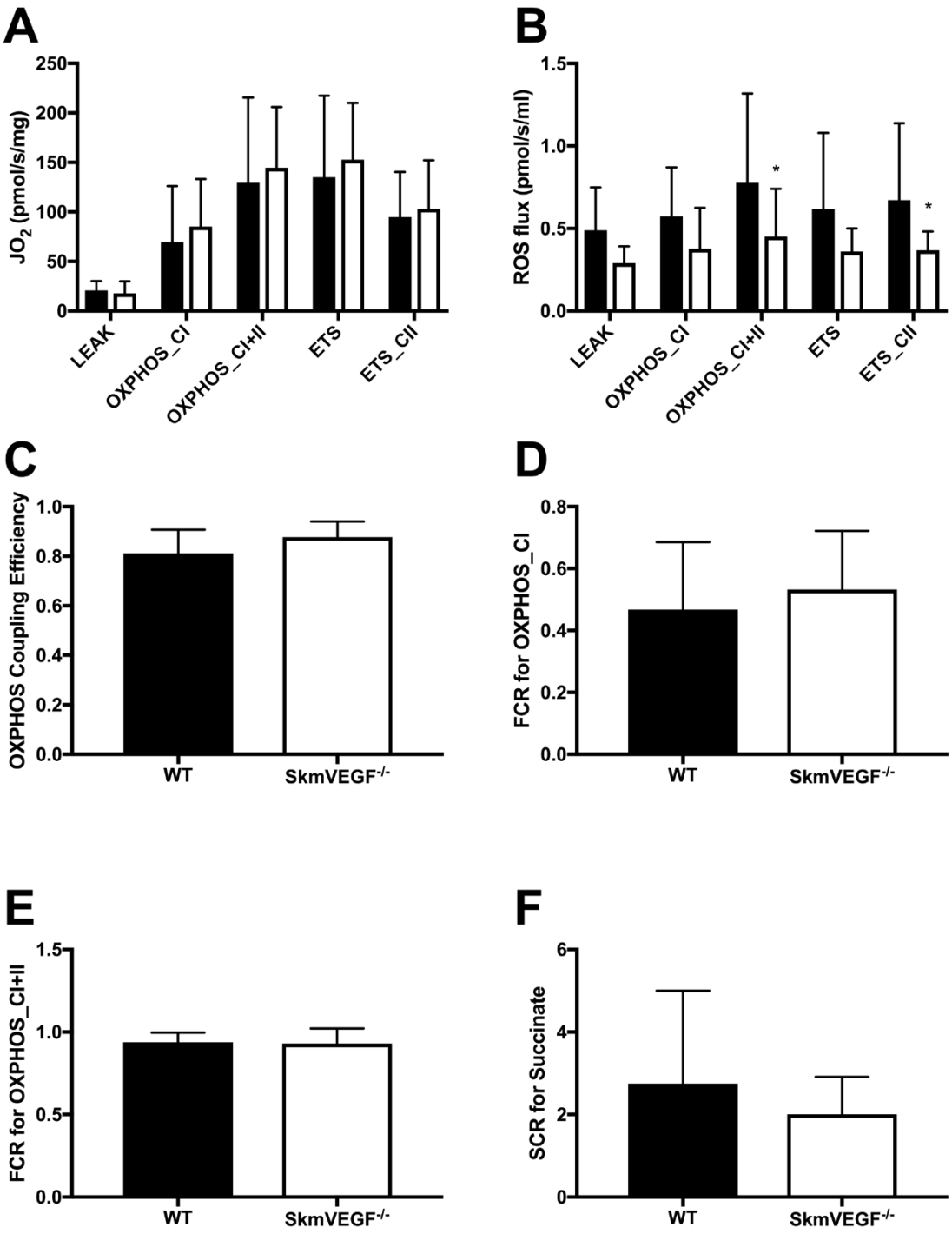
A
JO2 (pmol/s/mg)
250
200
150
100
50
0
LEAK
OXPHOS_CI
OXPHOS_CI+II
ETS
ETS_CII
B
ROS flux (pmol/s/ml)
1.5
1.0
0.5
0.0
*
*
LEAK
OXPHOS_CI
OXPHOS_CI+II
ETS
ETS_CII
C
OXPHOS Coupling Efficiency
1.0
0.8
0.6
0.4
0.2
0.0
WT
SkmVEGF-/-
D
FCR for OXPHOS_CI
0.8
0.6
0.4
0.2
0.0
WT
SkmVEGF-/-
E
FCR for OXPHOS_CI+II
1.5
1.0
0.5
0.0
WT
SkmVEGF-/-
F
SCR for Succinate
6
4
2
0
WT
SkmVEGF-/-

Figure 5.